

# Prompt fission $\gamma$ -ray characteristics from neutron-induced fission on $^{239}\text{Pu}$ and the time-dependence of prompt $\gamma$ -ray emission

Angélique Gatera<sup>1,2</sup>, Alf Göök<sup>2</sup>, Franz-Josef Hambsch<sup>2</sup>, André Moens<sup>2</sup>, Andreas Oberstedt<sup>3</sup>, Stephan Oberstedt<sup>2,\*</sup>, Goedele Sibbens<sup>2</sup>, David Vanleeuw<sup>2</sup>, and Marzio Vidali<sup>2</sup>

<sup>1</sup>Ghent University, Department of Physics and Astronomy, Proeftuinstraat 86, 9000 Ghent, Belgium

<sup>2</sup>European Commission, DG JRC, Directorate G - Nuclear Safety and Security, G.2 SN3S, 2440 Geel, Belgium

<sup>3</sup>Extreme Light Infrastructure - Nuclear Physics (ELI-NP) / Horia Hulubei National Institute for Physics and Nuclear Engineering (IFIN-HH), 077125 Bucharest-Magurele, Romania

**Abstract.** Recent years have seen an increased interest in prompt fission  $\gamma$ -ray (PFG) measurements motivated by a high priority request of the OECD/NEA for high precision data, mainly for the nuclear fuel isotopes  $^{235}\text{U}$  and  $^{239}\text{Pu}$ . Our group has conducted a PFG measurement campaign using state-of-the-art lanthanum halide detectors for all the main actinides to a precision better than 3%. The experiments were performed in a coincidence setup between a fission trigger and  $\gamma$ -ray detectors. The time-of-flight technique was used to discriminate photons, traveling at the speed of light, and prompt fission neutrons. For a full rejection of all neutrons below 20 MeV, the PFG time window should not be wider than a few nanoseconds. This window includes most PFG, provided that no isomeric states were populated during the de-excitation process. When isomeric states are populated, PFGs can still be emitted up to 1  $\mu\text{s}$  after the instant of fission or later. To study these  $\gamma$ -rays, the detector response to neutrons had to be determined and a correction had to be applied to the  $\gamma$ -ray spectra.

The latest results for PFG characteristics from the reaction  $^{239}\text{Pu}(n_{th},f)$  will be presented, together with an analysis of PFGs emitted up to 200 ns after fission in the spontaneous fission of  $^{252}\text{Cf}$  as well as for thermal-neutron induced fission on  $^{235}\text{U}$  and  $^{239}\text{Pu}$ . The results are compared with calculations in the framework of the Hauser-Feshbach Monte Carlo code CGMF and FIFRELIN.

## 1 Introduction

After almost 80 years since the discovery of nuclear fission the underlying process is still not understood in sufficient details. There are many fundamental questions still to be answered, touching both the nuclear energy as well as the basic science community. The first community is represented by the OECD Nuclear Energy Agency (NEA) [1], who expressed the need for more accurate fission cross-section and fragment yield data for safety assessments of Generation-IV reactor systems [2]. The second community, dealing with nuclear theory and the modeling of the fission process, are aiming at a detailed description of the nuclear fission process with predictive power for the observables, e.g.

\*e-mail: [stephan.oberstedt@ec.europa.eu](mailto:stephan.oberstedt@ec.europa.eu)

fragment yield and total kinetic energy distributions. Of particular interest is the understanding of the de-excitation mechanism of very neutron-rich isotopes that are produced in nuclear fission and how the excitation energy is shared between the two fission fragments.

The energy released in nuclear fission is distributed in kinetic and excitation energy of the two fragments. The excitation energy manifests itself in fragment deformation and intrinsic excitation energy. The first step of fission fragment de-excitation takes place at a very early stage after scission through the successive emission of neutrons and  $\gamma$  rays. In nuclear applications the prompt energy release by neutrons and  $\gamma$  rays accounts for about 5% of the total prompt heat set free in nuclear fission. Per definition prompt fission  $\gamma$ -rays may be emitted still after several microseconds, i.e. before the onset of  $\beta$  decay. Those isomeric  $\gamma$ -rays may be used to detect and identify actinides, that recently gained considerable attention for developing techniques to prevent illicit trafficking of fissile material.

The advances made in recent editions of various fission models presently on the market [3–9] require precise experimental data on prompt fission neutron and  $\gamma$ -ray emission as input parameters. For example multiplicity, average energy per particle and total dissipated energy per fission, preferably as function of fission-fragment mass and total kinetic energy, are key input to benchmark nuclear fission models attempting to describe the competition between prompt neutron and  $\gamma$ -ray emission.

Some years ago, a collaboration of scientists from JRC Geel (the former JRC IRMM) and other institutes took the lead in establishing a dedicated measurement programme on prompt fission neutron [10, 11] and fission  $\gamma$ -ray characteristics [12–17] responding to a high-priority data request of the OECD NEA. Here, we report about our most recent measurement of prompt fission  $\gamma$ -ray spectral PFGS characteristics from neutron-induced fission on  $^{239}\text{Pu}$ . Those results made it necessary to verify previous results obtained for prompt fission  $\gamma$ -ray characteristics from neutron-induced fission on  $^{235}\text{U}$  [14]. In addition, we present first results on time-dependent PFGS emission.

In the following we recall the essential information about our experimental technique and the applied data analysis, before we present and discuss our experimental results.

## 2 Experiment technique and data analysis

Experiments with spontaneously fissioning isotopes were performed at the JRC Geel, thermal-neutron induced fission at the cold-neutron beam at the Budapest Research Reactor. As detector for fission fragments a Frisch-grid ionization chamber (FGIC) is used providing a detection efficiency close to 100%. Counting gasses with a electron drift velocity of at least  $10^5$  m/s were used,  $\text{CH}_4$  and  $\text{Ar-CF}_4(10\%)$ , to minimize the  $\alpha$ -fission and the fission-fission pile-up rate. In combination with current sensitive pre-amplifiers the signal length was kept to 300 ns and 150 ns, respectively.

As  $\gamma$  ray detectors we used three cerium-doped lanthanum-bromide ( $\text{LaBr}_3:\text{Ce}$ ) detectors of size 51 mm  $\times$  51 mm (diameter  $\times$  length), which provided the best timing and energy resolution with sufficiently high detection efficiency. For the PFGS measurement on  $^{235}\text{U}$  a single 76 mm  $\times$  76 mm (diameter  $\times$  length)  $\text{LaBr}_3:\text{Ce}$  detector was used.

The data-acquisition system was based on 2-channel waveform digitizer cards with a sampling frequency of 400 MHz and a resolution of 14 bit [18].

Validation of our measurement setup and data analysis routines was done measuring prompt fission  $\gamma$ -rays from spontaneous fission of  $^{252}\text{Cf}$ . We used a  $^{252}\text{Cf}$  source with 11000 fission/s deposited on a 250 nm thick Ni-foil and placed in the FGIC on the central part of the cathode. In Table 1 we compare the average multiplicity,  $\bar{M}_\gamma$ , the mean photon energy,  $\epsilon_\gamma$ , and the average total  $\gamma$ -ray energy per fission,  $E_{\gamma,\text{tot}}$ , with our previous measurements as well as with data from literature. The validation of our method reflects in a reproduction of our previous results for  $\bar{M}_\gamma$ ,  $\epsilon_\gamma$  and  $E_{\gamma,\text{tot}}$  [12, 19] within 1%, 1.3% and 2.7%, respectively.

**Table 1.** Validation of our measurement setup and data analysis routines was done on spontaneous fission of  $^{252}\text{Cf}$ . The previous results on  $\overline{M}_\gamma$ ,  $\epsilon_\gamma$  and  $E_{\gamma,tot}$  [12, 19] are reproduced within 1%, 1.3% and 2.7%, respectively.

Results	Detector	$\overline{M}_\gamma$ (per fission)	$\epsilon_\gamma$ (MeV)	$E_{\gamma,tot}$ (MeV)	Energy range (MeV)
This work	LaBr <sub>3</sub> :Ce (Q489)	8.32 ± 0.10	0.83 ± 0.02	6.89 ± 0.11	0.1 – 7.0
This work	LaBr <sub>3</sub> :Ce (Q491)	8.41 ± 0.11	0.81 ± 0.02	6.80 ± 0.11	0.1 – 7.0
This work	LaBr <sub>3</sub> :Ce (5414)	8.35 ± 0.10	0.81 ± 0.02	6.78 ± 0.10	0.1 – 7.0
This work	LaBr <sub>3</sub> :Ce (5415)	8.44 ± 0.12	0.81 ± 0.02	6.82 ± 0.11	0.1 – 7.0
This work	Sum spectrum	8.38 ± 0.11	0.81 ± 0.02	6.82 ± 0.10	0.1 – 7.0
Billnert	LaBr <sub>3</sub> :Ce	8.30 ± 0.06	0.80 ± 0.01	6.64 ± 0.07	0.1 – 6.0

The  $^{239}\text{Pu}$  target was electrodeposited on 25  $\mu\text{m}$  thick Al. The 2 cm large circular spot contained 430  $\mu\text{g}$  high-purity  $^{239}\text{Pu}$  (99.97%) leading to a fission rate of  $4.4 \times 10^4/\text{s}$ .

A thorough investigation of the detector response in a setup with a FGIC using the Geant4 code [21, 22] revealed an underestimation of the backscatter contribution to the response, possibly leading to an overestimation of the  $\gamma$ -ray yield below 300 keV. This required a verification of our results on PFGS from thermal-neutron induced fission on  $^{235}\text{U}$  [14]. Therefore, we added a  $\gamma$ -ray detector to the SCINTIA array [11], an instrument dedicated to measure prompt-neutron spectral data on  $^{235}\text{U}$  at thermal and resolved-resonance energies. The  $^{235}\text{U}$  target was a circular 7 cm diameter spot of 67.2  $\mu\text{gU}/\text{cm}^2$   $\text{UF}_4$  (99.94%  $^{235}\text{U}$  vacuum-evaporated onto a 27  $\mu\text{g}/\text{cm}^2$  polyimide foil plated with 50  $\mu\text{g}/\text{cm}^2$  Au. The average fission rate was about 4.5/s.

For the investigation of time-dependent PFG emission neutron -  $\gamma$  separation via their characteristic time-of-flight is no longer sufficient. It requires the determination of the detector response to fast neutrons. In our case this will manifest in the detection of  $\gamma$ -rays following the inelastic scattering of prompt fission neutrons essentially on  $^{79,81}\text{Br}$  and  $^{139}\text{Ce}$  from the scintillation material, and on  $^{27}\text{Al}$  from the detector encapsulation. In a first approach the Geant4 simulation was performed time-integrated. As input to Geant4 we used prompt fission neutron spectra from the ENDF/B-VII.1 nuclear data library [20] keeping the same geometry as previously defined for the simulation of the  $\gamma$  response of our detectors. The simulated response is then subtracted from the time-integrated PFG spectrum and compared with the PFG spectrum as obtained within the prompt time window from  $-3$  to 3 ns.

### 3 Experimental results and consequences for future evaluations

In Fig. 1 the emission spectra from the reaction  $^{239}\text{Pu}(n_{th}, f)$  is shown in logarithmic scale for all three detectors together with the emission spectrum obtained from the sum of the three measured spectra. In the inset a zoom into the energy range below 800 keV is shown in linear scale. For the detector with serial No. 5415 a dip between 200 and 400 keV is visible, whose origin is not yet explained. However, this does not compromise the significance of the spectral characteristics. Our spectral data essentially confirms the PFGS characteristics of Verbinski et al. [23] and shows the deficiency of the spectral data from Ref. [24] at energies below 300 keV (see Fig. 2). For details we refer to Ref. [27].

Model calculations performed with the Monte-Carlo codes FIFRELIN [25] (green dashes) and CGMF [26] (black dots) are in very good agreement with our results.

With an average total prompt  $\gamma$ -ray energy released per fission,  $E_{\gamma,tot}$ , the result from Verbinski et al. [23] is confirmed within the uncertainty ( $1\sigma$ ). This means that the observed excess in the  $\gamma$  heating does not originate from deficient PFGS data from thermal-neutron induced fission of  $^{240}\text{Pu}^*$ . All numerical details may be found in Table 1 of Ref. [27].

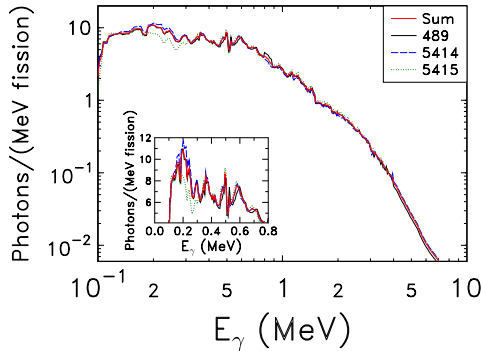


**Figure 1.** Prompt fission  $\gamma$ -ray spectra from thermal-neutron induced fission on  $^{239}\text{Pu}$  shown in logarithmic scale, taken with three different 51 mm  $\times$  51 mm (diameter  $\times$  length) cerium-doped (5%)  $\text{LaBr}_3$  detectors (serial numbers given). Depicted are the individual emission spectra and the one drawn from the sum of the three measured spectra. The inset shows a zoom-in on the low-energy region in linear scale.

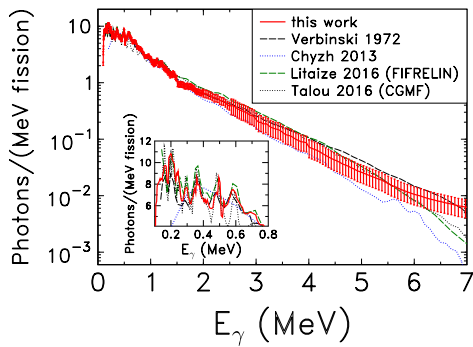


**Figure 2.** Prompt fission  $\gamma$ -ray spectra from thermal-neutron induced fission on  $^{239}\text{Pu}$  (red line with error bars) compared with data from Verbinski et al. [23] and Chyzh et al. [24]. We also show recent calculations performed with the Monte-Carlo codes FIFRELIN [25] and CGMF [26]. The inset shows a zoom-in on the low-energy region in linear scale.

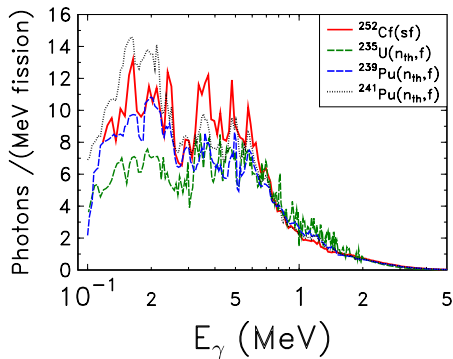


**Figure 3.** Summary of prompt fission  $\gamma$ -ray spectra for all fission reactions investigated by our collaboration (logarithmic energy scale). The spectral data for the reaction  $^{235}\text{U}(n_{th}, f)$  are from this work. The changing yields at different  $\gamma$  energies reflect the variation in the pre-neutron fission fragment yield distributions.

The PFGS of our verification run on thermal-neutron induced fission on  $^{235}\text{U}$  is shown in Fig. 3 as the green dashed line. Not only the photon yield below  $E_\gamma = 300$  keV is here drastically reduced, also all depicted PFG spectra - taken from all fission reactions investigated by our collaboration - reflect consistently the variations in the corresponding pre-neutron fragment mass yield distributions confirming the validity of the present detector response matrix. The comparison of our spectra also teaches us that the PFG spectrum for the reaction  $^{241}\text{Pu}(n_{th}, f)$ , which was measured under the same conditions as the one for  $^{235}\text{U}(n_{th}, f)$ , needs to be unfolded with the new response matrix.

Last but not least, we present our first results on time-dependent emission of prompt fission  $\gamma$ -rays or *late-time emission*, here for the thermal-neutron induced fission on  $^{239}\text{Pu}$ . As input for the

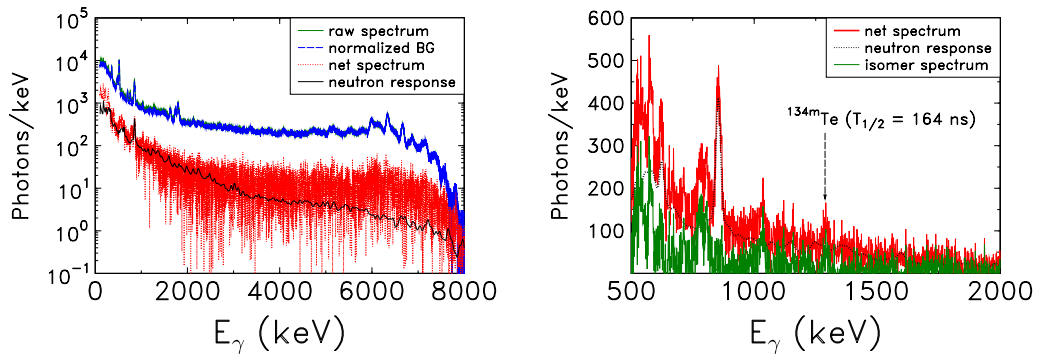


**Figure 4.** *Left part:* neutron response of a 51 mm × 51 mm (diameter × length) LaBr<sub>3</sub>:Ce(5%) (black line); the dotted (red) line is the net spectrum obtained as difference between the raw and the normalized background (BG) spectrum; *right part:* part of the isomer spectrum integrated between 3 and 200 ns obtained as difference between the net spectrum (red) and the neutron response spectrum (black dotted line). The proof of principle is given by the  $\gamma$  transition from the 1<sup>st</sup> excited state to the ground-state,  $E_\gamma = 1279.11$  keV, following the decay of the isomeric level in  $^{134m}\text{Te}$  ( $E^* = 1691.34$  keV).

**Table 2.** Prompt fission  $\gamma$ -ray emission as a function of time relative to the instant of fission in the thermal-neutron induced fission of  $^{240}\text{Pu}^*$ ; the data are for the detector with serial No. Q489. The cumulated multiplicity,  $\overline{M}_\gamma$ , is compared to calculations with the CGMF code [26].

time bin (ns)	$\overline{M}_\gamma$ (this work) (per fission)	$\overline{M}_\gamma$ [26] (per fission)
-3, 3	$7.27 \pm 0.11$	7.10
-3, 240	$7.66 \pm 0.12$	7.53

Geant4 simulations the prompt fission neutron spectrum from Ref. [20] was used. In the upper part of Fig. 4 the simulated detector response of our 51 mm × 51 mm LaBr<sub>3</sub>:Ce detectors is shown (black line) together with the integral raw spectrum (green line), the normalized background spectrum (blue dashed line) and the background-corrected total prompt fission  $\gamma$ -ray spectrum. The transition from the 1<sup>st</sup> excited to the ground state in  $^{27}\text{Al}$  is visible at  $E_\gamma = 843$  keV.

In the lower part of Fig. 4 the net spectrum (red) is shown together with the neutron response (dotted black) and the difference of the two, i.e. the isomer spectrum (green). The figure shows a  $\gamma$  energy range, which includes the transition from the isomer level in the fission product  $^{134m}\text{Te}$ , that has a half-life  $T_{1/2} = 164$  ns.

From this spectrum the isomeric, or late-time, contribution to the PFGS characteristics is deduced. First, tentative, numerical values for the cumulated PFG multiplicity as a function of time after fission are summarized in Table 2 and compared to results from model calculations [26]. Our data lies systematically higher, but a difference of 3% may, at the present stage, be considered as reasonable agreement.

## 4 Summary and outlook

During the last decade we conducted prompt fission  $\gamma$ -ray spectral measurements on a series of major and minor actinide samples, i.e.  $^{235}\text{U}(\text{n}_{\text{th}},\text{f})$ ,  $^{239,241}\text{Pu}(\text{n}_{\text{th}},\text{f})$  and  $^{240,242}\text{Pu}(\text{sf})$ , respectively. Our measurement technique and data analysis was validated by several measurements of the spontaneous fission of  $^{252}\text{Cf}$  samples employing targets with different fission rates and various lanthanide-halide detectors. We noticed that the determination of the detector response is crucial for obtaining the correct spectral shape at low  $\gamma$ -ray energies. First measurements on thermal-neutron induced fission of  $^{236}\text{U}^*$  were repeated under different experimental conditions. The new spectral data shows that the previous data needs to be reanalyzed using a more realistic response function.

With the PFGS data from neutron-induced fission of  $^{240}\text{Pu}^*$  we finalized the OECD/NEA HPRL requests for thermal energies. We do not find significant differences of PFGS characteristics compared to e.g. Verbinski's data. We may, therefore, conclude that the observed underestimation of the prompt  $\gamma$  heating is due to either fast-neutron induced fission or photo-fission induced by  $\gamma$ -rays from neutron capture in the construction material around the nuclear core.

We started to investigate so-called *late-time emission* of prompt fission  $\gamma$ -rays, i.e. isomeric decay in a time window adjacent to the prompt window,  $\Delta t = \pm 3$  ns, extending up to 240 ns in case of  $^{240}\text{Pu}^*$ . A first global assessment of the neutron response of our  $\text{LaBr}_3:\text{Ce}(5\%)$  detectors was done using Geant4. A comparison with the CGMF code shows global agreement.

In future we plan dedicated experiments in order to determine the time-dependent PFG emission in greater detail.

## References

- [1] Nuclear Data High Priority Request List of the NEA (Req. ID: H.3, H.4), <http://www.nea.fr/html/dbdata/hprl/hprlview.pl?ID=421> and <http://www.nea.fr/html/dbdata/hprl/hprlview.pl?ID=422>
- [2] G. Rimpault, in Proceedings of the Workshop on Nuclear Data Needs for Generation IV, April 2005, edited by P. Rullhusen (World Scientific, Singapore, 2006), p. 46
- [3] B. Becker, P. Talou, T. Kawano, Y. Danon, I. Stetcu, Phys. Rev. C **87**, 014617 (2013)
- [4] O. Litaize, D. Regnier, O. Serot, Phys. Proc. **59**, 89 (2014)
- [5] P. Talou, T. Kawano, I. Stetcu, R. Vogt, J. Randrup, Nucl. Data Sheets **118**, 227 (2014)
- [6] O. Serot, O. Litaize, D. Regnier, Phys. Proc. **59**, 132 (2014)
- [7] I. Stetcu, P. Talou, T. Kawano, M. Jandel, Phys. Rev. C **90**, 024617 (2014)
- [8] K.-H. Schmidt, B. Jurado, Ch. Amouroux, JEFF-Report 24, Data Bank, Nuclear Energy Agency, OECD (2015)
- [9] R. Vogt, J. Randrup, Nucl. Data Sheets **118**, 220 (2014)
- [10] N. Kornilov, F.-J. Hamsch, I. Fabry, S. Oberstedt, T. Belgya, Z. Kis, L. Szentmiklosi, S. Simakov, Nucl. Sci. Eng. **165**, 117 (2010)
- [11] A. Göök, F.-J. Hamsch, S. Oberstedt, Eur. J. Phys. Web of Conf. **111**, 05001 (2016)
- [12] R. Billnert, F.-J. Hamsch, A. Oberstedt, S. Oberstedt, Phys. Rev. C **87**, 024601 (2013)
- [13] M. Lebois, J.N. Wilson, P. Halipré, A. Oberstedt, S. Oberstedt, P. Marini, C. Schmitt, S.J. Rose, S. Siem, M. Fallot, A. Porta, A.-A. Zakari, Phys. Rev. C **92**, 034618 (2015)
- [14] A. Oberstedt, T. Belgya, R. Billnert, R. Borcea, T. Bryś, W. Geerts, A. Göök, F.-J. Hamsch, Z. Kis, T. Martinez, S. Oberstedt, L. Szentmiklosi, K., Takács, and M. Vidali, Phys. Rev. C. **87**, 051602(R) (2013)

- [15] S. Oberstedt, A. Oberstedt, A. Gatera, A. Göök, F.-J. Hamsch, A. Moens, G. Sibbens, D. Vanleeuw, and M. Vidali, *Phys. Rev. C* **93**, 054603 (2016)
- [16] S. Oberstedt, R. Billnert, F.-J. Hamsch, M. Lebois, A. Oberstedt, and J.N. Wilson, *Eur. Phys. J. A* **51**, 178 (2015)
- [17] S. Oberstedt, R. Billnert, T. Belgya, T. Bryś, W. Geerts, C. Guerrero, F.-J. Hamsch, Z. Kis, A. Moens, A. Oberstedt, G. Sibbens, L. Szentmiklosi, D. Vanleeuw, and M. Vidali, *Phys. Rev. C* **90**, 024618 (2014)
- [18] <http://spdevices.com/index.php/adq214>
- [19] A. Oberstedt, R. Billnert, F.-J. Hamsch, and S. Oberstedt, *Phys. Rev. C* **92**, 014618 (2015)
- [20] ENDF/B-VII.1 Evaluated Nuclear Data File, MF = 5, MT = 18 (2011), <http://www.nndc.bnl.gov/exfor/endf00.jsp>
- [21] S. Agostinelli and the Geant4 collaboration, *Nucl. Inst. Meth. A* **506**, 250 (2003)
- [22] PENELOPE11 Computer code, <http://www.oecd-nea.org/tools/abstract/detail/nea-1525>
- [23] V.V. Verbinski, H.Weber, and R.E. Sund, *Phys. Rev. C* **7**, 1173 (1973)
- [24] A. Chyzh, C.Y. Wu, E. Kwan, R.A. Henderson, J.M. Gostic, T.A. Bredeweg, R.C. Haight, A.C. Hayes-Sterbenz, M. Jandel, J.M. O'Donnell, and J.L. Ullman, *Phys. Rev. C* **85**, 021601 (2012)
- [25] O. Litaize and O. Serot, FIFRELIN ver. 2016 (private communication)
- [26] P. Talou, T. Kaweno, I. Stetcu, J.P. Lestone, E. McKigney, and M.B. Chadwick, *Physical Review C* **94**, 064613 (2016)
- [27] A. Gatera, T. Belgya, W. Geerts, A. Göök, F.-J. Hamsch, M. Lebois, B. Maróti, A. Moens, A. Oberstedt, S. Oberstedt, F. Postelt, L. Qi, L. Szentmiklosi, G. Sibbens, D. Vanleeuw, M. Vidali, and F. Zeiser, *Phys. Rev. C* **95**, 064609 (2017)

